1C3-4

Pedestrian Classification Based on Radial Velocity Features of UWB Doppler Radar Images

Kenshi Saho [1], Takuya Sakamoto [1], Toru Sato [1], Kenichi Inoue [2], Takeshi Fukuda [2]
[1] Graduate School of Informatics, Kyoto University
Kyoto 606–8501, Japan ksaho@sato-lab.0t0.jp
[2] Advanced Technology Research Laboratories, Panasonic Corporation
Kyoto 619–0237, Japan

1. Introduction

Imaging and identification of people using low-complexity radar is a promising technique for surveillance systems. Many studies have been conducted on the development of target identification methods using time-frequency micro-Doppler signatures [1]- [4]. These conventional methods can realize classification of motion types such as running, sitting, walking and walking without arm-motion. However, for accurate classification using these methods, reliable and long-term data or time-consuming procedures are needed, and their accuracy and real-time capability are thus inadequate. To resolve this problem, the use of shape and motion information is an option. For this purpose, we have proposed an ultra wide-band (UWB) Doppler radar imaging method with interferometry [5]. This method achieved adequate and real-time 3-dimensional human imaging with three receiving antennas in a realistic situation. This paper presents the imaging results on a variety of pedestrians using the UWB Doppler radar imaging method, and proposes their classification parameters based on a radial velocity feature of the estimated image. We experimentally verify that an effective classification for three types of pedestrians is achieved.

2. UWB Doppler Radar Imaging Method

Figure 1 shows the system model. We set a transmitting antenna Tx and three receiving antennas Rx_1, $_2$, and $_3$ in the xz plane. The central point of the antennas is $(0, 0, z_c)$. The transmitting signal is a UWB pulse with a center frequency of f_0. The bandwidth is W, which corresponds to a downrange resolution of $\Delta R = c/2W$, where c is the speed of light. We acquire the received signal $s_{ij}(t)$ in range j using receiver i.

The UWB Doppler radar imaging method separates multiple scattering centers with time-frequency distribution, and estimates the position of each separated scattering center with interferometry [5]. The time-frequency distribution $S_{ij}(t, v_\mathrm{d})$ is obtained using the sliding-window discrete Fourier transform (SDFT) of $s_{ij}(t)$, where v_d is the radial velocity determined by the Doppler frequency. We can separate multiple scattering centers by the differences in their radial velocities. Echo peaks with significant magnitude are extracted from $S_{ij}(t, v_\mathrm{d})$; these peaks correspond to the scattering centers on the target. We then estimate the positions of scattering centers which correspond to extracted peaks. The elevation direction-of-arrival (DOA) $\theta_\mathrm{EL}(t, v_{\mathrm{d}n})$ and azimuth DOA $\theta_\mathrm{AZ}(t, v_{\mathrm{d}n})$ of the n-th scattering center are determined using interferometry expressed by:

$$\theta_\mathrm{EL}(t, v_{\mathrm{d}n}) = \sin^{-1}\left[\frac{\angle S_{1k}(t, v_{\mathrm{d}n}) - \angle S_{3k}(t, v_{\mathrm{d}n})}{(2\pi d/\lambda)}\right], \tag{1}$$

$$\theta_\mathrm{AZ}(t, v_{\mathrm{d}n}) = \sin^{-1}\left[\frac{\angle S_{1k}(t, v_{\mathrm{d}n}) - \angle S_{2k}(t, v_{\mathrm{d}n})}{\{2\pi d \cos\theta_\mathrm{EL}(t, v_{\mathrm{d}n})/\lambda)\}}\right], \tag{2}$$

where λ is the wavelength and k is the range bin in which a target is detected. The distance R is estimated by finding the range that maximizes the echo intensity with a range interpolation method [5]. With

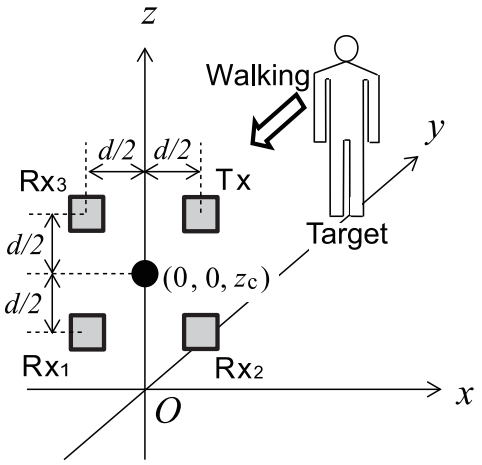

Figure 1: System model.

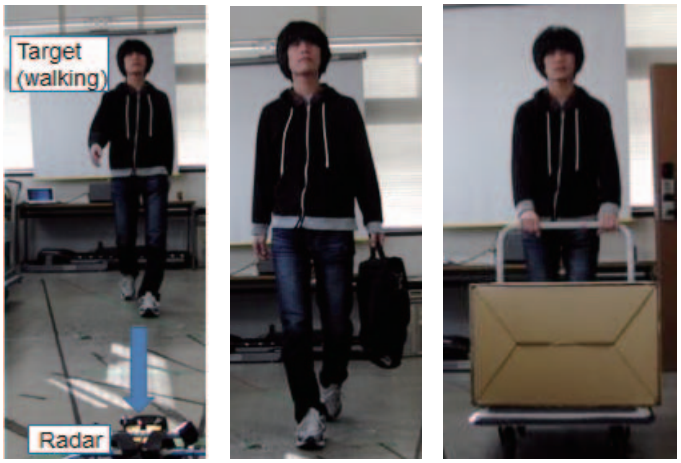

(a) Target A and experimental site (b) Target B (c) Target C

Figure 2: Experimental site and targets.

acquired distance and DOA, the position of each scattering center is determined by:

$$\mathbf{x}_{\mathrm{s}}(t, v_{\mathrm{d}n}) = \begin{bmatrix} x_{\mathrm{s}}(t, v_{\mathrm{d}n}) \\ y_{\mathrm{s}}(t, v_{\mathrm{d}n}) \\ z_{\mathrm{s}}(t, v_{\mathrm{d}n}) \end{bmatrix} = \begin{bmatrix} R(t, v_{\mathrm{d}n}) \cos\theta_{\mathrm{EL}}(t, v_{\mathrm{d}n}) \sin\theta_{\mathrm{AZ}}(t, v_{\mathrm{d}n}) \\ R(t, v_{\mathrm{d}n}) \cos\theta_{\mathrm{EL}}(t, v_{\mathrm{d}n}) \cos\theta_{\mathrm{AZ}}(t, v_{\mathrm{d}n}) \\ R(t, v_{\mathrm{d}n}) \sin\theta_{\mathrm{EL}}(t, v_{\mathrm{d}n}) + z_{\mathrm{c}} \end{bmatrix}. \tag{3}$$

In addition, we apply a false image rejection method [5] to the estimated $\mathbf{x}_{\mathrm{s}}(t, v_{\mathrm{d}n})$ to reduce the effect of interference between multiple scattering centers.

3. Imaging Examples and Discussion for a Variety of Pedestrians

In this section, we present the experiments which assume three types of pedestrian target: Target A is a normal pedestrian with swinging arms, Target B has a bag in his left hand, and Target C is a pedestrian carrying a box on a hand truck. Figure 2 shows pictures of the experimental site and the pedestrian targets. In all scenarios, a person with a height of 1.75 m walks from (x, y) =(0, 3.9 m) to (0, 1.5 m) with a gait cycle of 1.54 s and an average speed of 0.78 m/s. The radar parameters are d=3.5 cm, f_0=26.4 GHz, W=500 MHz, and ΔR=30 cm. Horn antennas are used with −3dB beamwidth of ± 11° in both the E- and H-planes. The interpulse period is 1.29 ms, and the window size for the SDFT is 165 ms. We take measurements at four antenna positions: z_{c}= 0.36, 0.83, 1.3 and 1.5 m, and imaging is performed by the superposition of the scattering centers estimated in each antenna position.

Figure 3 shows the frontal views of the estimated images corresponding to half a walking cycle. As shown in Fig. 3(a), the outline of the human shape is confirmed. Moreover, we can recognize from radial velocity information that the left leg and right arm have forward motion in this half cycle. Although Target B has nearly the same properties as Target A, the number of scattering centers corresponding to arms is relatively small. This is because his arm-swing amplitude is small because he is carrying the bag. We can see the scattering centers on the bag at approximately (x, z) =(0.25 m, 0.5 m) in Fig. 3(b). In Fig. 3(c), the scattering centers are concentrated in a relatively narrow region in terms of both the position and v_{d}. This is because the hand truck moves toward the radar with an approximately constant velocity.

As discussed above, the estimated images and their radial velocities have feature information on each pedestrian type. Here, we investigate the radial velocity feature of the imaging results. Figure 4 shows the power density for each (v_{d}, z) corresponding to Fig. 3. As shown in (a) and (b) of this figure, we can see significant peaks corresponding to the legs' motion near the floor. Moreover, at around z =1.3 m, the radial velocity spread which corresponds to the arms' motion is confirmed in Fig. 4(a). In contrast, the radial velocity spread of Target B for relatively large z is small compared with that of Target A because

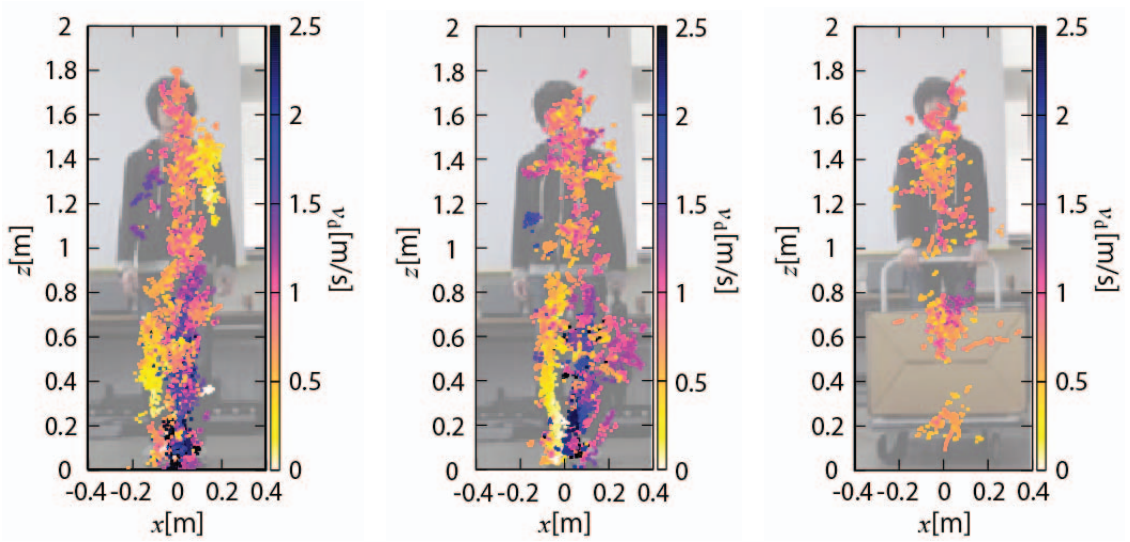

(a) Target A (b) Target B (c) Target C

Figure 3: Frontal view of the estimated image.

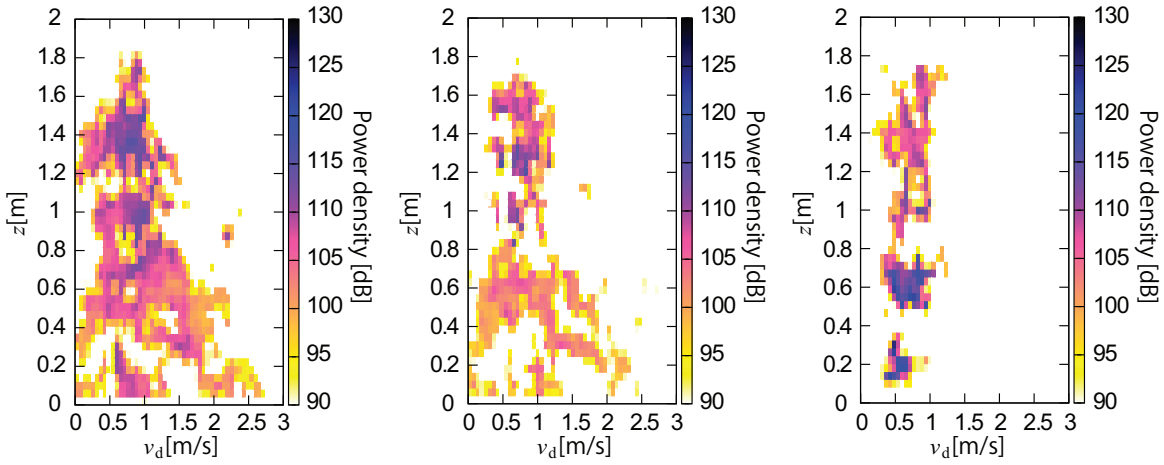

(a) Target A (b) Target B (c) Target C

Figure 4: Power density for each radial velocity and height.

of the bag. On the other hand, the radial velocity spread of Target C is small because of the constant speed of the hand truck.

4. Proposed Classification Parameters and Results

Based on the discussion in the previous section, we propose effective parameters for pedestrian classification using the radial velocity spread. We use the standard deviation of the radial velocity distribution in the relatively low z region, which is expressed as:

$$\sigma_{\mathrm{dl}} = \sqrt{\frac{1}{N'_{\mathrm{T}}}\sum_{i}^{N_{\mathrm{T}}} a_i^2 - \left[\frac{1}{N'_{\mathrm{T}}}\sum_{i}^{N_{\mathrm{T}}} a_i\right]^2}, \tag{4}$$

where

$$a_i = \begin{cases} v_{\mathrm{d}i} & (z_{si} < z_{\mathrm{l}}) \\ 0 & (\text{Otherwise}), \end{cases} \tag{5}$$

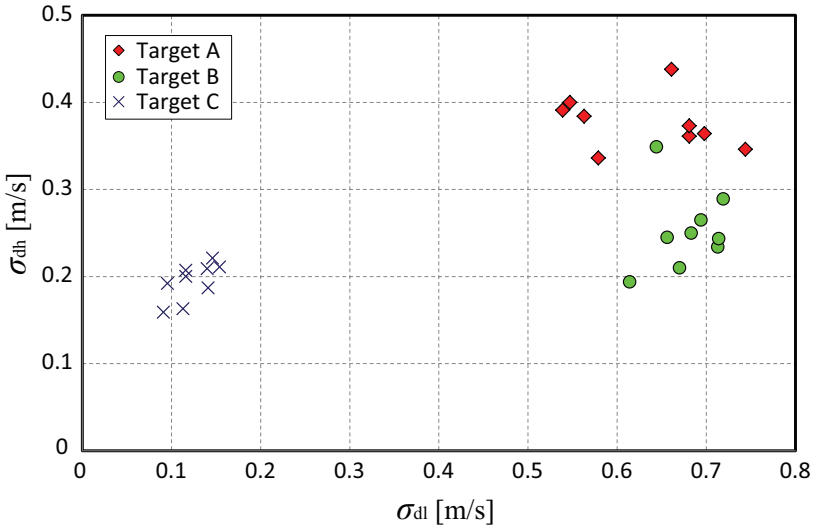

Figure 5: Estimation result of the proposed classification parameters.

v_{di} and z_{si} are i-th scattering center's v_d and z_s, N_T is the total number of estimated scattering centers, and N'_T is the number of scattering centers that satisfies $z_s < z_l$. Moreover, we use a standard deviation σ_{dh}, which is determined by the image that satisfies $z_s > z_h$ in the same way.

Figure 5 shows the estimation results of the proposed standard deviations for each target. Here, we use the data from half a walking cycle to estimate each point in this figure, and empirically set $z_l = 0.6$ m and $z_h = 1.0$ m. Although one σ_{dh} of Target B becomes relatively large, we can clearly recognize that there are three types of pedestrians, and can classify these targets easily.

5. Conclusions

This paper demonstrated the imaging and classification of three types of pedestrians using UWB Doppler radar. We proposed a method for their classification using the standard deviation of the radial velocity distribution of the estimated images. The experiments show that the proposed parameters achieved pedestrian classification in a realistic environment.

References

[1] I. Orovic, S. Stankovic, M. Amin, "A new approach for classification of human gait based on time-frequency feature representations", Signal Processing, Vol.91, No.6, pp.1448–1456, 2011.

[2] P. Lei, J. Wang, P. Guo, D. Cai, "Automatic classification of radar targets with micro-motions using entropy segmentation and timefrequency features" Int. J. Electron. Commun., Vol.65, pp.806–813, 2011.

[3] Y. Kim, H. Ling, "Through-wall human activities classification using support vector machine", IEEE Trans. Geoscie. Remote Sens., Vol.47, pp.1328–1337, 2009.

[4] D. P. Fairchild, R. M. Narayanan, "Human activity classification using Hilbert-Huang transform analysis of radar Doppler data", Proc. Society of Photo-Optical Instrumentation Engineers (SPIE) 8021, Florida, USA, 80210F, 2011.

[5] K. Saho, T. Sakamoto, T. Sato, K. Inoue, T. Fukuda, "Experimental Study of Real-Time Human Imaging Using UWB Doppler Radar Interferometry", Proc. 6th European Conf. on Antennas and Propagation (EuCAP2012), Prague, Czech Republic, M16-3, 2012.